Materials Science

Research article

Circular self-cleaning building materials and fabrics using dual doped TiO$_2$ nanomaterials

Evangelos Karagiannis*, Dimitra Papadaki* and Margarita N. Assimakopoulos

Physics Department, National and Kapodistrian University of Athens, Panepistimioupoli, Zografoy, Athens, MO 15784, Greece

* Correspondence: Email: evankara@phys.uoa.gr, dpapadaki@phys.uoa.gr.

Abstract: Nanostructured titanium dioxide (TiO$_2$) among other oxides can be used as a prominent photocatalytic nanomaterial with self-cleaning properties. TiO$_2$ is selected in this research, due to its high photocatalytic activity, high stability and low cost. Metal doping has proved to be a successful approach for enhancing the photocatalytic efficiency of photocatalysts. Photocatalytic products can be applied in the building sector, using both building materials as a matrix, but also in fabrics. In this study undoped and Mn-In, Mn-Cu, In-Ni, Mn-Ni bimetallic doped TiO$_2$ nanostructures were synthesized using the microwave-assisted hydrothermal method. Decolorization efficiency of applied nanocoatings on fabrics and 3-D printed sustainable blocks made from recycled building materials was studied, both under UV as well as visible light for Methylene Blue (MB), using a self-made depollution and self-cleaning apparatus. Nanocoated samples showed high MB decolorization and great potential in self-cleaning applications. Results showed that the highest MB decolorization for both applications were observed for 0.25 at% Mn-In doped TiO$_2$. For the application of 3-D printed blocks Mn-In and In-Ni doped TiO$_2$ showed the highest net MB decolorization, 25.1 and 22.6%, respectively. For the application of nanocoated fabrics, three samples (Mn-In, In-Ni and Mn-Cu doped TiO$_2$) showed high MB decolorization (58.1, 52.7 and 47.6%, respectively) under indirect sunlight, while under UV light the fabric coated with Mn-In and In-Ni doped TiO$_2$ showed the highest MB decolorization rate 26.1 and 24.0%, respectively.

Keywords: nanomaterials; TiO$_2$; doping; self-cleaning; anti-pollution; decolorization; circular building materials; fabrics

1. Introduction

Nanotechnology is bringing new materials and new possibilities to industries contributing to an improved living environment and comfort on a daily base. One of these is the construction industry, where nanotechnology can generate products with many unique characteristics that can improve the performance of current construction materials introducing new applications with enhanced sustainable properties [1]. New materials and products based on nanotechnology can be found in building matrices, coatings or insulating applications. Specifically, lighter and stronger structural composites, low maintenance coatings, better cementitious materials, lower thermal transfer rate of fire retardant and insulation, self-cleaning windows, smog-eating concrete, antimicrobial coatings, photovoltaic devices that converts sunlight to electricity and many other advances [2–5]. The incorporation of recycled construction materials and 3-D printing in construction industry is a further step towards innovation and sustainability. Nonetheless the building industry accounts for 40% of the energy consumption and 50% of the greenhouse gas emissions in Europe [6].

Within the EU more than 50% of all extracted materials are attributed to buildings. The exploitation of natural resources is a serious threat to the natural, social and economic systems in the EU. A transition to both a deep and circular renovation process with the use of recycled materials in the construction industry is necessary to meet the challenge of decarbonization [7]. The use of recycled materials in the construction industry totally alters the value chain linked to all stages of intervention in existing buildings, making the operations sustainable in social, environmental and economic terms [8,9]. Furthermore, the use of innovative, cost effective and time efficient technologies such as 3-D printing technologies, provide state of the art ways to improve the quality of new constructions by minimizing the chance of errors, using highly precise material deposition, reducing on-site construction time by operating at a constant rate and reducing the costs connected to the design and management of buildings and infrastructures, combined with reduced labor requirements, and minimal material usage [10–12]. Cleaning of surfaces may be disadvantageous involving the removal of the protection layer, changing the color of pigmented elements, leaving behind chemical contaminants and increasing the risk of rain penetration. Moreover, the pollutants have a major effect on building structures and interior decorative items. For example, black particles and tobacco smoke cause soiling of light-colored surfaces and sulfates/nitrates because of the acid rains enhancing the surface recession [13,14]. A solution to this is the use of photocatalytic nanomaterials. Photocatalytic titanium dioxide nanoparticles with self-cleaning properties can be used as coatings on building blocks or pavements, but also on interior decorative items such as ceiling panels, curtains and wallpapers [15–19].

Nanostructured titanium dioxide is one of the most popular photocatalyst with the characters of long-term photostability, non-toxicity and low-cost availability [20]. However, TiO_2 due to wide band-gap (3.2 eV for anatase) exhibits high photocatalytic activity under ultraviolet illumination. There are efforts regarding the improvement of TiO_2 photocatalysis by shifting the band gap energy so that it is active under visible light by doping or combining TiO_2 with different non-metal or transition metal ions [21–25]. Also, TiO_2 can be used as photocatalytic products with antimicrobial properties, or air purifier, waste water treatment cleaning and water disinfection [26–29].

Specifically, a way to enhance visible light photocatalytic performance of TiO_2 nanoparticles is by combining them with conjugated polymers. These nanoparticles can be employed as an efficient photocatalyst to treat the organic pollutants and remove hazardous materials [30,31]. Moreover,

doping TiO$_2$ with Nd^{3+} exhibits simultaneous photocatalytic activity and NIR photoluminescent emission, suitable for applications such as environmental remediation, smart materials, and display technologies [32].

Nowadays the textile industry has become a significant contributor to water pollution, resulting in the generation of huge volumes of wastewater [33]. In the perspective of the state of the art for improved TiO$_2$ based photocatalyst materials through various modification strategies many studies aim to apply them for the removal of contaminants of emerging concerns (CECs), dye degradation and antibacterial activity [33–36].

In this study, TiO$_2$ dopped with a variety of dopants is being assessed both under UV and Vis light and its depollution is measured on circular 3D printed building materials as well as in fabrics.

2. Materials and methods

2.1. Microwave oven synthesized undoped and doped TiO$_2$ nanoparticles

Undoped and Mn-In, Mn-Cu, In-Ni, Mn-Ni bimetallic doped TiO$_2$ nanostructures were synthesized using the microwave-assisted hydrothermal method. The microwave-assisted hydrothermal method has unique advantages of uniform and rapid heating in comparison with the conventional one. In addition, this method can significantly reduce the reaction time, leading to the fast crystallization with a narrow size distribution and high purity [37–39].

Solution (0.1 M) of Titanium (IV) oxysulfate-sulfuric acid hydrate (99.95% trace metals basis, Sigma Aldrich), was dissolved into 250 mL of distilled water and were mixed under fast stirring for 45 min. The obtained solution was transferred into four Teflon vessels and irradiated in an advanced flexible microwave synthesis platform (Milestone flexiWAVE), using the high-pressure setup at 120 °C for 30 min (max 1500 Watt). When the reaction was finished and cooled to room temperature, the precipitate was collected, centrifuged (1000 rpm for 2 min) and washed several times with ethanol and distilled water (Figure 1).

Mn-In, Mn-Cu, In-Ni and Mn-Ni doped TiO$_2$ nanostructures were prepared following the same experimental procedure used to prepare undoped TiO$_2$ by also adding into the precursor solution, 0.25 at% of indium(III) nitrate hydrate (In(NO$_3$)$_3$·H$_2$O, 99.9% Sigma-Aldrich) with nickel(II) nitrate hexahydrate (Ni(NO$_3$)$_2$·6H$_2$O, ≥97.0%, Honeywell FlukaTM), manganese(II) nitrate tetrahydrate (Mn(NO$_3$)$_2$·4H$_2$O, ≥97.0%, Honeywell FlukaTM) with indium(III) nitrate hydrate, manganese(II) nitrate tetrahydrate with copper(II) nitrate trihydrate (Cu(NO$_3$)$_2$·3H$_2$O, 99–104%, Honeywell FlukaTM) and manganese(II) nitrate tetrahydrate with nickel(II) nitrate hexahydrate, respectively.

In all cases the microwave was programmed with a first temperature ramp where the target temperature was reached after 15 min. All products were kept at room temperature overnight and totally dried using an oven at 100 °C for 1 h.
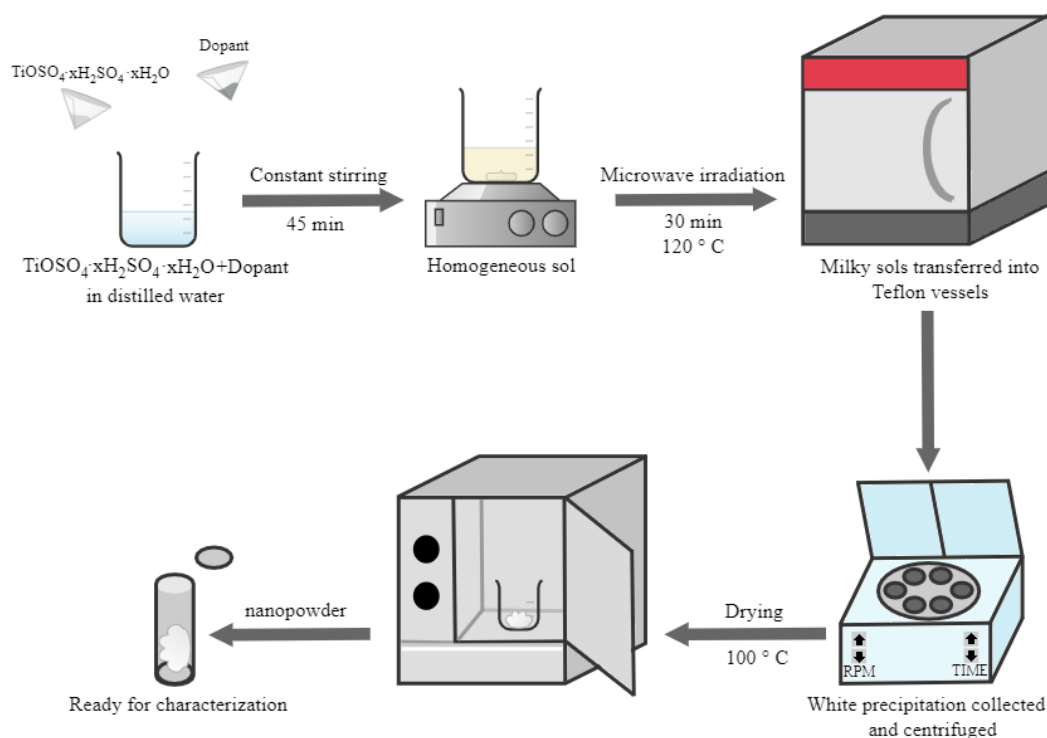
Figure 1. Schematic representation of the synthetic procedure employed for the preparation of doped and undoped TiO$_2$ nanostructures.

2.2. Characterization techniques

Their crystallographic structure was examined using a Siemens D5000, X-ray diffractometer, equipped with a Cu-Kα (λ = 0.15405 nm) monochromatic radiation source. The specific surface area of the samples was examined by nitrogen (N$_2$) physisorption using a Micromeritics' Gemini VII 2390 Surface Area Analyzer. The samples were prior degassed at 100 °C for 2 h under continuous nitrogen gas flow using a Micromeritics' FlowPrep 060, in order to remove moisture.

2.3. Synthesis of blocks and fabrics

A mix of equal amounts of recycled concrete aggregate and recycled gypsum powder, supplied by ATTICA RECYCLING CD & EW SA, was used for the 3-D printing of blocks (Figure 2a). The dimensions of each block were 5 × 5 × 1 cm and printed with a Z Corporation 3-D printer (ZPrinter 310 Plus). In order to minimize the inconsistencies between the powder samples a reference block was simultaneously printed with the test-sample. Thus, 3-D printed a pair of blocks was delivered, one block served as reference (blank) and one as the test-bed for the circular building materials layered on the top with the nanocoating. The fabric that was used is based on 98% cotton and 2% viscose and is depicted with a grey color (Figure 2b). The dimensions of each fabric sample were 7 × 7 cm. The fabric mass per unit area was 125 g per square meter.

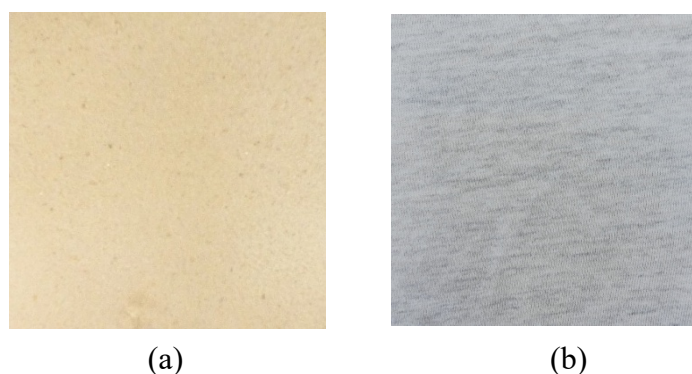<center>(a)   (b)</center>

Figure 2. Initial state of (a) 3-D printed blocks and (b) fabric samples.

2.4. Decolorization experiments

Decolorization of applied coatings was evaluated by the use of a self-made apparatus for the decolorization of Methylene Blue (MB). Degradation of pollutant was assessed by a colorimetric method and by a Varian CARY-5000 DRA 2500 UV-VIS-NIR Spectrophotometer. The color analysis was performed using the CIELAB model.

2.4.1.   Preparation of 3-D printed blocks

The 3-D printed blocks were separated into five pairs of blocks, each one consisting of the nanocoated block and its reference (blank) block (Table 1). Each nanocoated block was covered with 0.1 g of a photocatalytic nanomaterial as slurry, which was left to dry. In order to evaluate the decolorization effect, the 3-D printed blocks were dip-coated with a MB solution and after exposed to UV light.

Table 1. 3-D printed block samples and the method of coating.

Nanocoated ID	Nanomaterial	Coating	Reference ID	Coating
TiOP	Undoped TiO_2	0.004 g/cm^2	Ref1	Blank
MnInP	Mn-In/TiO_2		Ref2	
MnNiP	Mn-Ni/TiO_2		Ref3	
InNiP	In-Ni/TiO_2		Ref4	
MnCuP	Mn-Cu/TiO_2		Ref5	

2.4.2.   Experimental set up

The exposure to UV light was held into a handmade photocatalytic apparatus (Figure 3). The apparatus consists of a wooden box, which is equipped with two Prinz UV Test lamps (4W, UV-A 366 nm) and a base for supporting the pair of blocks. The horizontal distance of the blocks with the lamps was 3 cm, the height of the base was 3.5 cm while the distance between lamps was 4 cm and between blocks 2 cm.

The decolorization of the MB dye applied to the surfaces of the blocks was monitored by the use of chromatic measurements before UV irradiation and after 1 and 2 h of exposure.

(a)   (b)

Figure 3. Handmade photocatalytic apparatus for blocks.

2.5. Preparation of fabrics

For the decolorization of applied coatings on fabric six samples were used, one for each nanomaterial and one blank as reference (Table 2). Each nanocoated fabric sample was covered with 4 wt% of a photocatalytic nanomaterial as slurry, then pressed with a roller and left to dry. The fabrics were dip-coated with a MB solution and left to dry under indirect sunlight for a day.

Table 2. Fabric samples and the method of coating.

Sample ID	Nanomaterial	Coating
TiOF	Undoped TiO_2	4 wt%
MnInF	Mn-In/TiO_2	
MnNiF	Mn-Ni/TiO_2	
InNiF	In-Ni/TiO_2	
MnCuF	Mn-Cu/TiO_2	

2.5.1. Experimental set up

The decolorization of the MB dye applied to the surfaces of the fabrics was monitored by the use of chromatic measurements before and after the exposure to indirect sunlight. After that the samples were exposed to UV irradiation. For this purpose, the initial photocatalytic apparatus was modified. The base was replaced by a thread and three hooks to hold each fabric sample in its place (Figure 4). The horizontal distance of the fabrics with the lamps was 4 cm, lamps and fabric samples were respectively 8 cm and 12 cm above the surface of the box, while the distance between lamps was 12 cm and between fabrics 8 cm. The decolorization of the MB dye applied to the surfaces of the fabrics was monitored by a Cary 5000 UV-VIS-NIR spectrophotometer before UV irradiation and after 1 and 2 h of exposure.
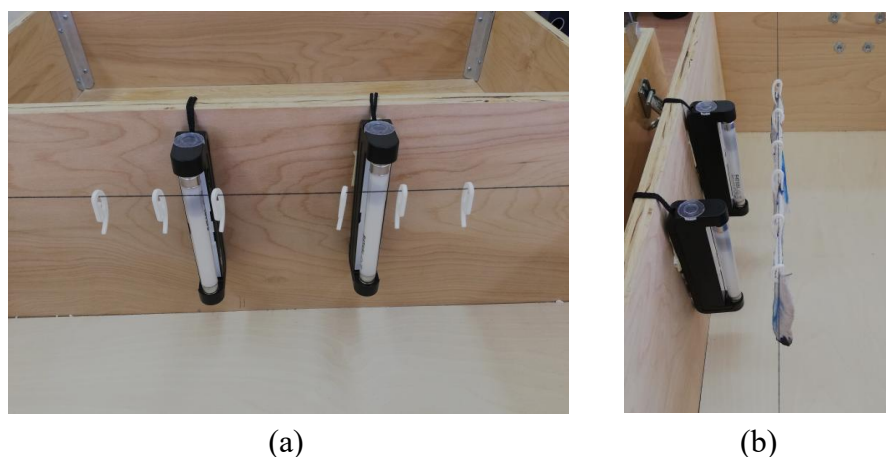
(a)   (b)

Figure 4. Handmade photocatalytic apparatus for fabrics.

3. Results and discussion

3.1. Structural analysis using X-ray diffraction

The X-ray diffraction patterns of undoped and Mn-In, Mn-Cu, In-Ni and Mn-Ni doped TiO_2 nanostructures (Figure 5) only exhibited patterns assigned to the TiO_2 anatase phase (JCPDS file card No.-01-071-1166). No signal from the crystalline phase containing metal or metal oxide of the doping elements could be observed indicating that the dopant ions have been successfully doped into the TiO_2 lattice. Furthermore, careful analyses of the main peak (101) of the XRD patterns (Figure 5, inset) indicated a slight shift to the higher angle side for Mn-In, Mn-Cu, In-Ni and mainly for Mn-Ni doped TiO_2 nanoparticles.

By comparing the ionic radius values [40–43] of Ti^{4+} (0.68 Å) to that of In^{3+} (0.81 Å), Mn^{2+} (0.80 Å), Ni^{2+} (0.72Å) and Cu^{2+} (0.73Å), we hypothesize that some of the doping elements were incorporated into the structures of TiO_2, by replacing titanium or oxygen atoms and some occupies the interstitial position, which induced a perturbation in anatase crystal structure [44,45]. Replacement by In^{3+}, Mn^{2+}, Ni^{2+} and Cu^{2+} dopant ions may cause expansion/compression of the unit cell resulting to variation in various parameters including micro-strain due to lattice mismatch and distortion. The increase in lattice (micro) strain can be explained by the dopant substitution on the oxygen sites of TiO_2 surface.
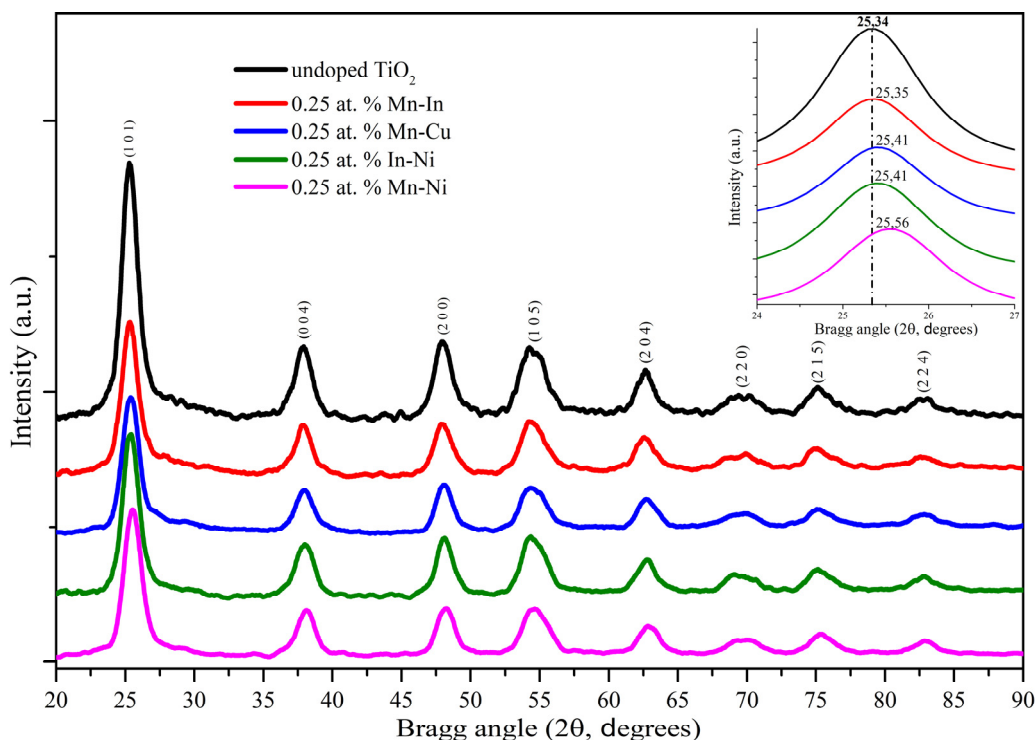
Figure 5. X-ray diffraction (XRD) patterns of undoped and doped TiO$_2$. The inset shows the peak (101) of doped and undoped TiO$_2$.

The lattice constants a, b and c have been calculated from the XRD patterns using the Eq 1 [46].

$$\frac{1}{d^2} = \frac{(h^2 + k^2)}{a^2} + \frac{l^2}{c^2} \tag{1}$$

where h, k, and l are the Miller indices; a and c are the lattice constants; and d is the interplanar spacing, which can be determined from Bragg's law

$$2 \cdot d \cdot \sin\theta = n \cdot \lambda \tag{2}$$

The lattice parameters were calculated for undoped and Mn-In, Mn-Cu, In-Ni and Mn-Ni doped TiO$_2$ nanostructures (Table 3). It is apparent that the lattice parameters are decreased upon addition of different types of dopant ions.

The average crystallite sizes of undoped and doped TiO$_2$ samples were also determined (Table 3) by measuring the full width at half-maximum of the prominent peak (101) of anatase, using the Debye-Scherrer method Eq 3 [47].

$$D = \frac{K \cdot \lambda}{\beta_{hkl} \cdot \cos\theta} \tag{3}$$

where D is the average crystallite size; K is the shape factor, usually taken as 0.9; λ is the wavelength of radiation in nanometer ($\lambda_{CuK\alpha} = 0.15405$ nm); θ is the diffracted angle of the peak; β_{hkl} is the full width at half maximum of the peak in radians.

It is well known that the Debye-Scherrer formula provides only the lower limit of crystallite size [48]. Therefore, the structural properties and XRD peak broadening of the samples were investigated by Size-Strain Plot (SSP) method to evaluate the crystallite sizes and lattice strains [44,45,49].

Table 3. Crystallite size, strain and lattice parameters for the undoped and Mn-In, Mn-Cu, In-Ni and Mn-Ni doped TiO_2 nanostructures.

Sample	2θ [101] (deg)	Lattice parameters a = b (Å)	c (Å)	Unit cell volume ($Å^3$)	d spacing [101] (nm)	Crystallite size Scherrer	SSP	Strain (10^{-3})
undoped TiO_2	25.34	3.786	9.490	136.04 ± 0.07	3.512 ± 0.001	6.0	6.2	3.54
0.25 at% Mn-In	25.35	3.785	9.489	135.98 ± 0.07	3.510 ± 0.001	6.0	6.4	3.75
0.25 at% Mn-Cu	25.41	3.780	9.470	135.30 ± 0.07	3.502 ± 0.001	6.1	6.4	3.45
0.25 at% In-Ni	25.41	3.778	9.466	135.10 ± 0.07	3.503 ± 0.001	5.9	6.1	3.11
0.25 at% Mn-Ni	25.56	3.771	9.439	134.25 ± 0.07	3.482 ± 0.001	5.8	6.0	3.64

3.1.1. Size-Strain Plot (SSP) method

Size-strain parameters can be obtained from the SSP method. This has a benefit that less importance is given to data from reflections at high angles, where the accuracy and precision are less, than that in lower angles. This is because, at higher angles, XRD data are of lower quality and peaks are generally highly overlapped at higher diffracting angles [50].

In this method, it is assumed that the crystallite size profile is described by a Lorentzian function and that the strain profile is described by a Gaussian function [50–52]. Hence we have,

$$(d_{hkl} \cdot \beta_{hkl} \cdot \cos\theta)^2 = \frac{K \cdot \lambda}{D} \cdot (d_{hkl}^2 + \beta_{hkl} \cdot \cos\theta) + \frac{\varepsilon^2}{4} \qquad (4)$$

The Size-Strain plots of undoped and bimetallic doped TiO_2 nanostructures (Figure 6) are plotted with the term $(d_{hkl} \cdot \beta_{hkl} \cdot \cos\theta)^2$ along Y-axis against the term $(d_{hkl}^2 + \beta_{hkl} \cdot \cos\theta)$ along x-axis as per Eq 4. The size and strain for each sample have been calculated from the slope and intercept of the graphs, respectively (Table 3).

The average crystallite size calculated by Size-Strain Plot method was found to increase from 6.2 nm for the undoped TiO_2 to 6.4 nm for the Mn-In, Mn-Cu doped TiO_2 and decrease to 6.1 and 6.0 nm for the In-Ni, Mn-Ni doped TiO_2, respectively. Moreover, the lattice strain ε was found to increase with the Mn-In, Mn-Ni doping and decrease with the Mn-Cu, In-Ni doping. In this work, average crystallite sizes calculated from the Debye-Scherrer method and SSP method is found to be comparable with each other.
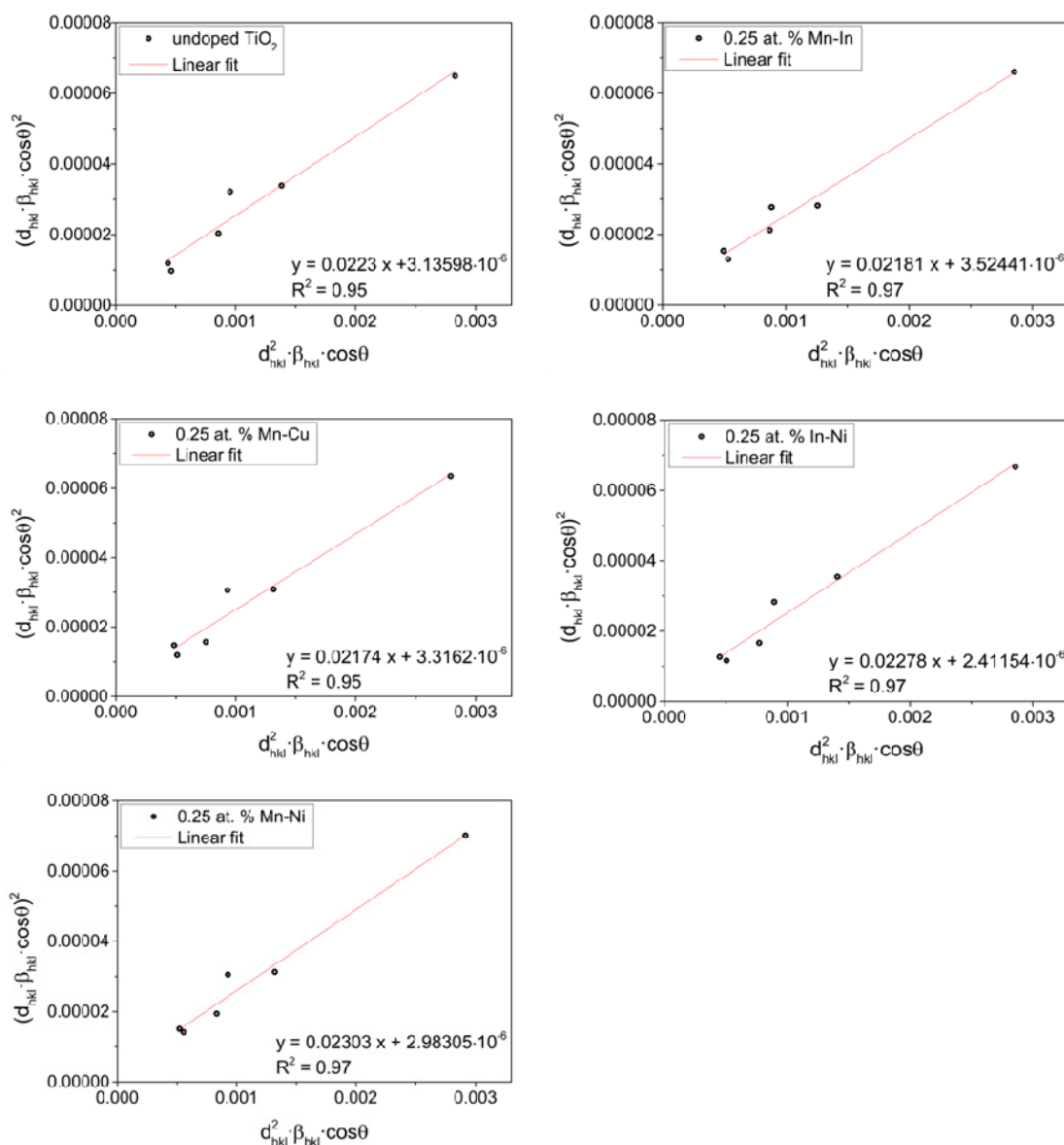
Figure 6. Size Strain Plots (SSP) graph of undoped and Mn-In, Mn-Cu, In-Ni and Mn-Ni doped TiO_2 nanostructures.

3.2. BET surface area of doped and undoped TiO_2 nanostructures

The photocatalytic activity of nanoparticles is highly related to their surface properties such as surface area. The selection of dopants plays a significant role on the surface area of the nanomaterial. More specifically, undoped TiO_2 showed the surface area of 96.7 m^2/g, the TiO_2 doped with Mn-Cu and In-Ni revealed higher surface area of 98.8 and 98.4 m^2/g respectively, while Mn-In and Mn-Ni displayed lower surface areas accounting to 81.5 and 94.1 m^2/g respectively (Figure 7). Lower surface area may be justified by aggregation of nanostructures or because of partial pore blockages from dopants and framework defects [53]. It is well demonstrated that the nature of dopant ions is affecting the BET-specific surface area. Each curve has a point of inflection called a "knee" around $P/P_0 = 0.1$ (Figure 7). This point indicates that monolayer adsorption is complete and multilayer

formation starts to take place. Over this point the adsorbed volume was increased predominantly, which means that there are also mesopores on doped and undoped TiO$_2$ nanostructures [54].
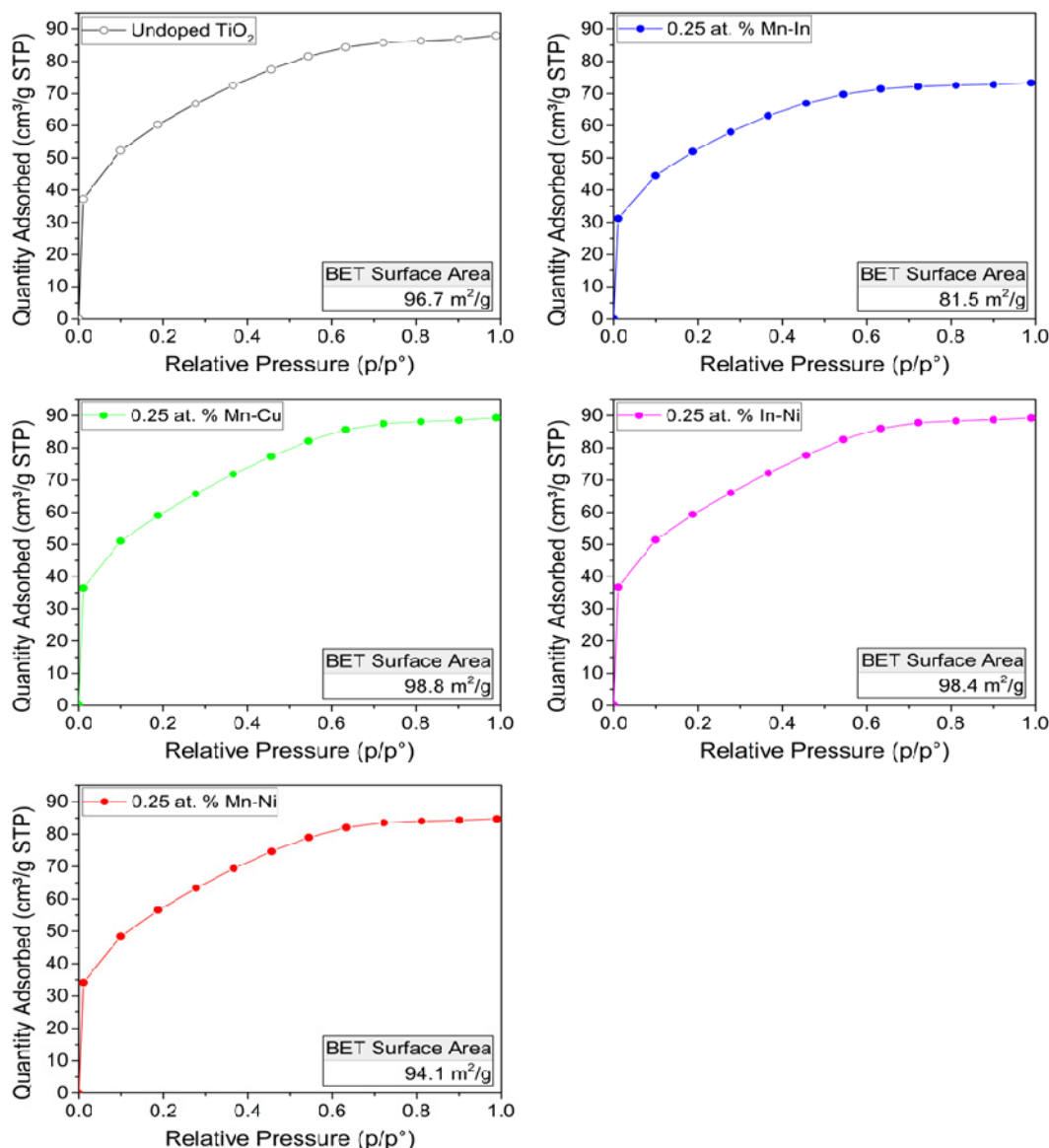

Figure 7. N$_2$ adsorption isotherms for undoped and Mn-In, Mn-Cu, In-Ni and Mn-Ni doped TiO$_2$ nanostructures.

3.3. Decolorization of methylene blue

3.3.1. Application of 3-D printed blocks

The decolorization of the MB dye applied to the surfaces of the 3-D printed blocks under UV exposure, was monitored by the use of chromatic measurements. For better evaluation of the initial conditions of the substrate and the effect of color differences that may occur between the analyzed surfaces before the test, the decolorization values (D) were normalized with respect to the original aspect of substrate before deposition of MB dye. The decolorization D has been calculated using Eq 5.

$$D(\%) = \frac{\Delta E(t)}{\Delta E(0)} \cdot 100 \tag{5}$$

where $\Delta E(t)$ is the total color difference of chromatic coordinates at a specific time under UV irradiation with respect to the sample before the UV exposure, and $\Delta E(0)$ is the total color difference of the sample prior to UV exposure with respect to the sample before the deposition of MB dye (original block).

The decolorization of nanocoated 3-D printed blocks, after 120 min of UV irradiation, were found to be 44.5, 31.6, 34.4, 34.1 and 19.6% for sample TiOP, InNiP, MnInP, MnNiP and MnCuP, respectively (Figure 8). While the decolorization of the reference 3-D printed blocks, after 120 min of UV irradiation, were 23.8, 9.3, 16.0, 9.0 and 7.7% for sample Ref1, Re2, Ref3, Ref4 and Ref5, respectively (Figure 8). The decolorization of reference 3-D printed blocks is mainly caused by the sorption (absorption and adsorption) of MB dye onto the blocks.
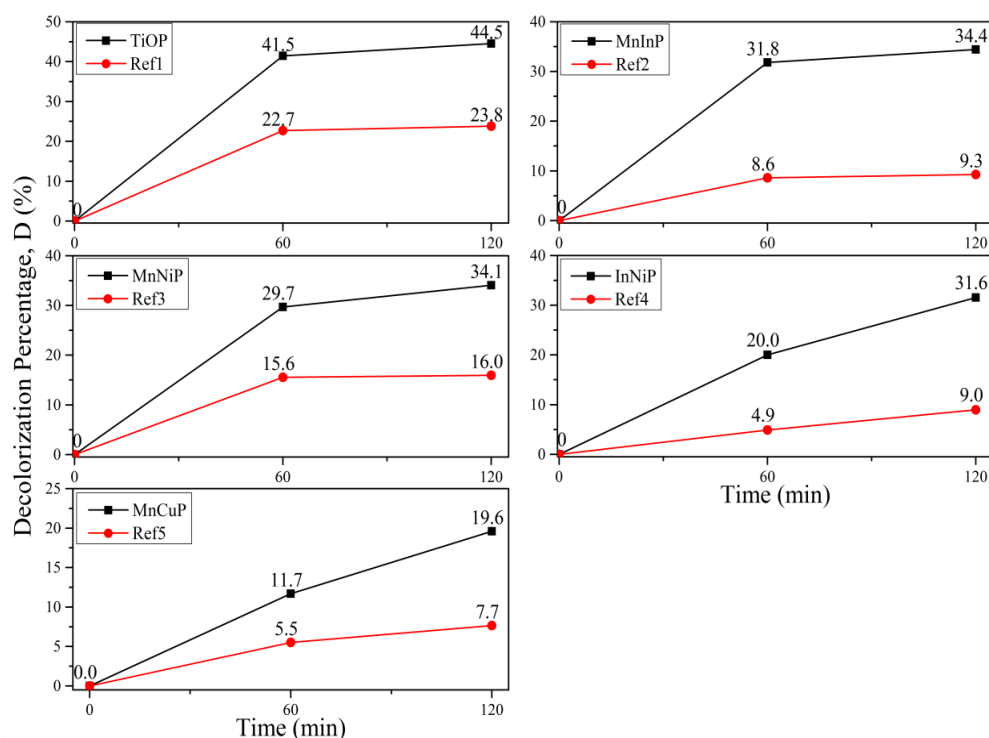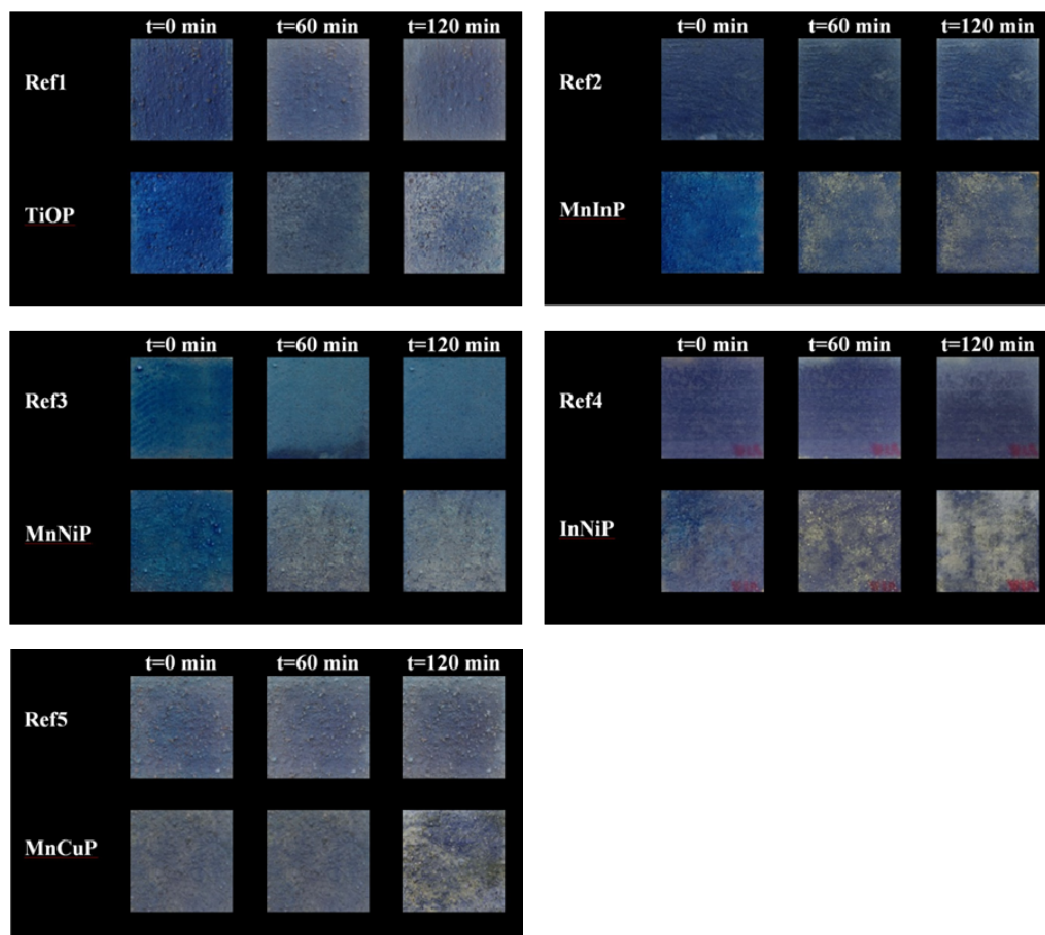

Figure 8. Decolorization of each pair of 3-D printed blocks under UV light. The black and red lines describe the decolorization of nanocoated and reference blocks, respectively.

It is important to compare each pair of blocks in order to distinguish the sorption processes from the decolorization of each nanomaterial applied. The net decolorization (ND = $D_{Nanocoated} - D_{Reference}$) of blocks caused by the nanomaterials used for the coating of the 3-D printed blocks, after 2 h of UV light exposure were found to be 20.7, 25.1, 18.1, 22.6 and 12.0% for sample TiOP, InNiP, MnInP, MnNiP and MnCuP, respectively (Table 4). The sample coated with 0.25 at% Mn-In doped TiO_2 showed the highest decolorization rate of MB dye (Figure 9).

Table 4. Net decolorization of 3-D printed blocks after 60 and 120 min of UV light exposure.

Time (min)	ND_{TiOP} (%)	ND_{MnInP} (%)	ND_{MnNiP} (%)	ND_{InNiP} (%)	ND_{MnCuP} (%)
60	18.8	23.2	14.1	15.1	6.2
120	20.7	25.1	18.1	22.6	12.0

Figure 9. Pairs of 3-D printed blocks at the beginning of the MB decolorization test before UV exposure (t = 0) and after 60 and 120 min of UV irradiation.

3.3.2. Application of fabrics

Indirect sunlight exposure: For the case of indirect sunlight exposure, the decolorization percentage values of fabrics was calculated using the Eq 5. The decolorization of reference and nanocoated fabrics, after indirect sunlight exposure, are 10.8, 13.3, 52.7, 58.1, 18.6 and 47.6% for sample Ref, TiOF, InNiF, MnInF, MnNiF and MnCuF, respectively (Table 5).

Table 5. Decolorization (D) of reference and nanocoated fabrics after indirect sunlight exposure.

Exposure	D_{Ref} (%)	D_{TiOF} (%)	D_{InNiF} (%)	D_{MnInF} (%)	D_{MnNiF} (%)	D_{MnCuF} (%)
Indirect sunlight	10.8	13.3	52.7	58.1	18.6	47.6

The fabrics coated with Mn-In, In-Ni and Mn-Cu doping showed great decolorization under sunlight (Figure 10). The fabric coated with Mn-In doping showed the best decolorization of MB dye, 47.3% more than the decolorization of the reference fabric, while fabric coated with undoped TiO_2 showed the smallest decolorization, 2.5% more than the decolorization of the reference fabric.
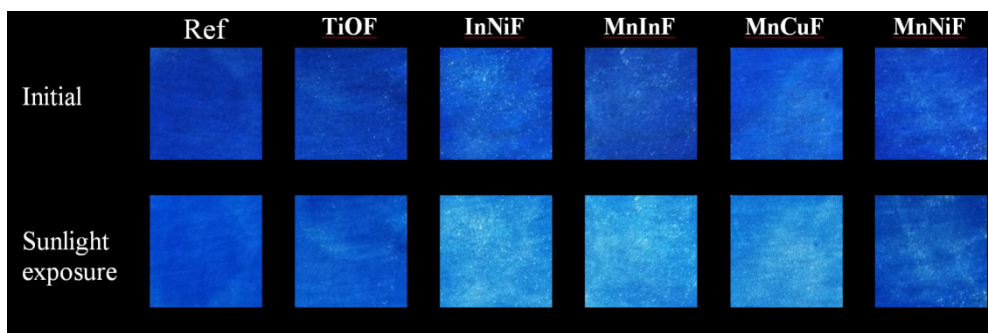

Figure 10. Reference and nanocoated fabrics at the beginning of the MB decolorization test before indirect sunlight exposure (Initial) and after exposure.

UV light exposure: The decolorization of fabrics was determined according to the Beer-Lambert law at the maximum absorbance ($\lambda_{max} = 670$ nm) using a UV-Vis spectrophotometer (Figure 11). The decolorization percentage D, was calculated using Eq 6.

$$D(\%) = \frac{(A_0 - A_t)}{A_0} \cdot 100 \qquad (6)$$

where A_0 and A_t stand for the absorbance before UV exposure and after a specific time under UV irradiation, respectively.

The decolorization of reference and nanocoated fabrics, after 120 min of UV irradiation, are 3.9, 15.9, 18.4, 26.1, 24.0 and 20.4% for sample Ref, TiOF, InNiF, MnInF, MnNiF and MnCuF, respectively (Table 6). The fabric coated with Mn-In doping showed the best decolorization, 22.2% more than the decolorization of the reference fabric, while the fabric coated with undoped TiO_2 and Mn-Ni doping showed the smallest decolorization, 12.0% and 14.5% more than the decolorization of the reference fabric, respectively (Table 6). The absorption spectra of fabrics nanocoated with Mn-Ni and Mn-Cu doping for higher wavelengths than 700 nm shows a maximum MB degradation, so we can assume that there will be no more decolorization after 120 min of UV irradiation (Figure 11).

Doping with different non-metal or transition metal ions can alter the crystallite size, lattice stress, porosity and surface area, affecting both energy gap and the recombination rate of photogenerated electron-hole pairs [43,55]. Undoped and Mn-In, Mn-Cu, In-Ni and Mn-Ni doped TiO_2 nanostructures were measured to have small crystallite size, large lattice strain and specific surface area. As a result to these characteristics, the nanocoatings showed high decolorization rate of MB dye. Mn-In doped TiO_2 nanocoatings showed the highest MB decolorization for both applications. The Mn-In doping of TiO_2 enhanced the MB decolorization rate in several ways. The lattice strain of Mn-In doped TiO_2 was measured to be the highest of all samples, while the surface area was the lowest probably due to partial pore blockages from dopants and framework defects [53]. These characteristics can reduce the adsorption strength of the MB onto the nanocoating, increasing the probability for the reactive oxygen species (ROS) to react with the MB since the nanocoating is

able to absorb light more effectively [56]. In addition, the excess surface defects created by Mn-In dopant can suppress the recombination rate of photogenerated electron-hole pairs, and then react with H_2O_2, OH^- and O_2 to generate OH and O_2^- radicals, which results in greater ROS generation [53].

Nanocoatings applied on the 3-D printed blocks are heavily substrate dependent [4]. Mn-Cu doped TiO_2 nanocoating couldn't incorporate successfully with the 3-D printed block. This was due to the appearance of a black-green coloration on block's surface probably produced by the photochemical reaction of copper. Furthermore, a poor dispersion of the Mn-Cu doped TiO_2 nanoparticles onto the block was observed. This problem can be solved with the help of any additional dispersing agent [4].

Compared to the application of 3-D printed blocks, nanocoatings showed better incorporation and dispersion onto the fabrics, resulting in the improvement of the MB decolorization rate. Doping enhanced the decolorization of MB under visible light, probably due to the reduction of the bandgap energy so that it can absorb energy from a major portion of visible light. Specifically, the fabrics coated with Mn-In, In-Ni and Mn-Cu doped TiO_2 showed great MB decolorization rate under indirect sunlight.
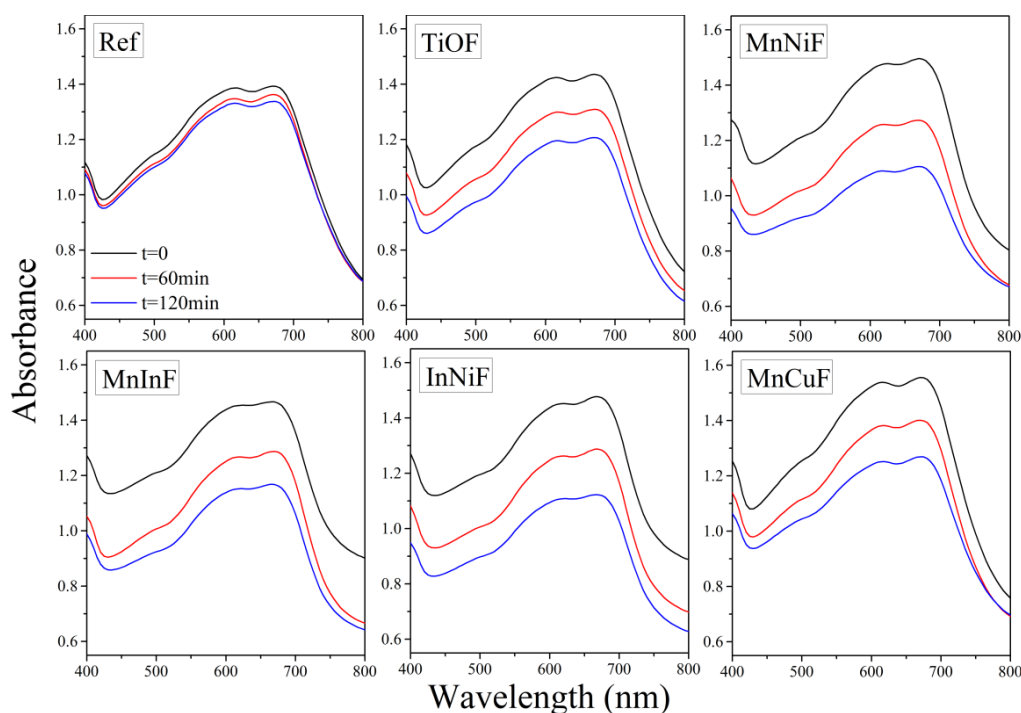

Figure 11. Absorption spectra of reference and nanocoated fabrics, before UV exposure (t = 0) and after 60 and 120 min of UV irradiation.

Table 6. Decolorization percentage of reference and nanocoated fabrics after 60 and 120 min of UV light exposure.

Time (min)	D_{Ref} (%)	D_{TiOF} (%)	D_{MnNiF} (%)	D_{MnInF} (%)	D_{InNiF} (%)	D_{MnCuF} (%)
60	2.2	8.8	9.9	14.9	12.8	12.2
120	3.9	15.9	18.4	26.1	24.0	20.4

4. Conclusions

In the present work, synthesis of undoped and Mn-In, Mn-Cu, In-Ni and Mn-Ni doped TiO_2 nanostructures were conducted and a low temperature anatase phase formation was successfully achieved using a green microwave assisted technique. The structure of nanoparticles was investigated by X-ray Diffraction analysis (XRD) and the specific surface area by the BET analysis. The XRD results revealed the shift in diffraction peak positions toward higher 2θ angles and the alteration in lattice parameters between undoped and Mn-In, Mn-Cu, In-Ni and Mn-Ni doped TiO_2 nanostructures, indicating TiO_2 lattice compression and production of lattice strain due to formation of defects on the TiO_2 surface. BET-specific area analysis revealed high surface area values for the undoped and Mn-In, Mn-Cu, In-Ni and Mn-Ni doped TiO_2 nanostructures associated with the microporous nature of the structures. The decolorization of the applied nanocoatings of 3-D printed blocks and fabrics was studied. Substrates were made of a mix of equal amounts of recycled concrete aggregate and recycled gypsum powder, while the fabrics mainly of cotton. Due to the high porosity of substrates, nanoparticles showed good adhesion. The nanocoated samples showed high MB decolorization and great potential in self-cleaning applications. The highest decolorization of MB for both applications were observed for 0.25 at% Mn-In doped TiO_2, probably because of the high lattice strain, which has been reported to be beneficial for photocatalytic activity with TiO_2. Moreover, the results of nanocoated fabrics under exposure to indirect sunlight provide a potential breakthrough in the modern textile industry.

Acknowledgments

Conflict of Interest

The authors declare that they have no known conflict for financial interests or personal relationships that could have appeared to influence the work reported in this paper.

References

1. Papadaki D, Kiriakidis G, Tsoutsos T (2018) Applications of nanotechnology in construction industry, In: Barhoum A, Abdel Salam HM, *Fundamentals of Nanoparticles*, Elsevier, 343–370. https://doi.org/10.1016/B978-0-323-51255-8.00011-2
2. Boostani H, Modirrousta S (2016) Review of nanocoatings for building application. *Procedia Eng* 145: 1541–1548. https://doi.org/10.1016/j.proeng.2016.04.194
3. Jesus MAMLD, Neto JTDS, Timò G, et al. (2015) Superhydrophilic self-cleaning surfaces based on TiO_2 and TiO_2/SiO_2 composite films for photovoltaic module cover glass. *Appl Adhes Sci* 3: 5. https://doi.org/10.1186/s40563-015-0034-4

4. Luna M, Delgado J, Gil M, et al. (2018) TiO$_2$–SiO$_2$ coatings with a low content of AuNPs for producing self-cleaning building materials. *Nanomaterials* 8: 177. https://doi.org/10.3390/nano8030177

5. Ünlü B, Özacar M (2020) Effect of Cu and Mn amounts doped to TiO$_2$ on the performance of DSSCs. *Sol Energy* 196: 448–456. https://doi.org/10.1016/j.solener.2019.12.043

6. Papadaki D, Foteinis S, Binas V, et al. (2019) A life cycle assessment of PCM and VIP in warm Mediterranean climates and their introduction as a strategy to promote energy savings and mitigate carbon emissions. *AIMS Mater Sci* 6: 944–959. https://doi.org/10.3934/matersci.2019.6.944

7. Tisov A, Kuusk K, Escudero MN, et al. (2020) Driving decarbonisation of the EU building stock by enhancing a consumer centred and locally based circular renovation process. *E3S Web of Conferences* 172: 18006. https://doi.org/10.1051/e3sconf/202017218006

8. Cheshire D (2019) *Building Revolutions: Applying the Circular Economy to the Built Environment*, RIBA Publishing. https://doi.org/10.4324/9780429346712

9. Mangialardo A, Micelli E (2018) Rethinking the construction industry under the circular economy: Principles and case studies. *International conference on Smart and Sustainable Planning for Cities and Regions*, 333–344. https://doi.org/10.1007/978-3-319-75774-2_23

10. Gao W, Zhang Y, Ramanujan D, et al. (2015) The status, challenges, and future of additive manufacturing in engineering. *Comput Aided Design* 69: 65–89. https://doi.org/10.1016/j.cad.2015.04.001

11. Xia M, Sanjayan J (2016) Method of formulating geopolymer for 3D printing for construction applications. *Mater Design* 110: 382–390. https://doi.org/10.1016/j.matdes.2016.07.136

12. Wangler T, Lloret E, Reiter L, et al. (2016) Digital Concrete: Opportunities and Challenges. *RILEM Tech Lett* 1: 67. https://doi.org/10.21809/rilemtechlett.2016.16

13. Mansour AMH, Al-Dawery SK (2018) Sustainable self-cleaning treatments for architectural facades in developing countries. *Alex Eng J* 57: 867–873. https://doi.org/10.1016/j.aej.2017.01.042

14. Li Y (2019) Study on the weathering mechanism and protection technology of stone archives. *IOP Conf Ser Mater Sci Eng* 490: 062032. https://doi.org/10.1088/1757-899X/490/6/062032

15. Janus M, Zając K (2019) Self-cleaning efficiency of nanoparticles applied on facade bricks, In: Pacheco-Torgal F, Diamanti MV, Nazari A, et al., *Nanotechnology in Eco-efficient Construction: Materials, Processes and Applications*, 2Eds., Elsevier, 591–618. https://doi.org/10.1016/B978-0-08-102641-0.00024-4

16. Diamanti MV, Pedeferri M (2019) Photocatalytic performance of mortars with nanoparticles exposed to the urban environment, In: Pacheco-Torgal F, Diamanti MV, Nazari A, et al., *Nanotechnology in Eco-efficient Construction: Materials, Processes and Applications*, 2Eds., Elsevier, 527–555. https://doi.org/10.1016/B978-0-08-102641-0.00022-0

17. Sikora P, Horszczaruk E, Rucinska T (2015) The effect of nanosilica and titanium dioxide on the mechanical and self-cleaning properties of waste-glass cement mortar. *Procedia Eng* 108: 146–153. https://doi.org/10.1016/j.proeng.2015.06.130

18. Abbas M, Iftikhar H, Malik M, et al. (2018) Surface coatings of TiO$_2$ nanoparticles onto the designed fabrics for enhanced self-cleaning properties. *Coatings* 8: 35. https://doi.org/10.3390/coatings8010035

19. Giesz P, Celichowski G, Puchowicz D, et al. (2016) Microwave-assisted TiO$_2$: anatase formation on cotton and viscose fabric surfaces. *Cellulose* 23: 2143–2159. https://doi.org/10.1007/s10570-016-0916-z

20. Humayun M, Raziq F, Khan A, et al. (2018) Modification strategies of TiO$_2$ for potential applications in photocatalysis: a critical review. *Green Chem Letter Rev* 11: 86–102. https://doi.org/10.1080/17518253.2018.1440324

21. Nurdin M, Ramadhan LOAN, Darmawati D, et al. (2018) Synthesis of Ni, N co-doped TiO$_2$ using microwave-assisted method for sodium lauryl sulfate degradation by photocatalyst. *J Coat Technol Res* 15: 395–402. https://doi.org/10.1007/s11998-017-9976-8

22. Moma J, Baloyi J (2019) Modified titanium dioxide for photocatalytic applications, In: Khan SB, Akhta K, *Photocatalysts: Applications and Attributes*, IntechOpen. https://doi.org/10.5772/intechopen.79374

23. Maragatha J, Rajendran S, Endo T, et al. (2017) Microwave synthesis of metal doped TiO$_2$ for photocatalytic applications. *J Mater Sci-Mater El* 28: 5281–5287. https://doi.org/10.1007/s10854-016-6185-7

24. Singh I, Birajdar B (2017) Synthesis, characterization and photocatalytic activity of mesoporous Na-doped TiO$_2$ nano-powder prepared via a solvent-controlled non-aqueous sol-gel route. *RSC Adv* 7: 54053–54062. https://doi.org/10.1039/C7RA10108B

25. Qi H, Lee J, Wang L, et al. (2016) Photocatalytic performance of titanium dioxide nanoparticles doped with multi-metals. *J Adv Oxid Technol* 19: 302–309. https://doi.org/10.1515/jaots-2016-0214

26. Gnanaprakasam A, Sivakumar VM, Thirumarimurugan M (2015) Influencing parameters in the photocatalytic degradation of organic effluent via nanometal oxide catalyst: A review. *Indian J Mater Sci* 2015: 1–16. https://doi.org/10.1155/2015/601827

27. Colangiuli D, Calia A, Bianco N (2015) Novel multifunctional coatings with photocatalytic and hydrophobic properties for the preservation of the stone building heritage. *Constr Build Mater* 93: 189–196. https://doi.org/10.1016/j.conbuildmat.2015.05.100

28. Matoh L, Žener B, Korošec RC, et al. (2019) Photocatalytic water treatment, In: Pacheco-Torgal F, Diamanti MV, Nazari A, et al., *Nanotechnology in Eco-efficient Construction: Materials, Processes and Applications*, 2Eds., Elsevier, 675–702. https://doi.org/10.1016/B978-0-08-102641-0.00027-X

29. Janjua ZA (2019) Icephobic nanocoatings for infrastructure protection, In: Pacheco-Torgal F, Diamanti MV, Nazari A, et al., *Nanotechnology in Eco-efficient Construction: Materials, Processes and Applications*, 2Eds., Elsevier, 281–302. https://doi.org/10.1016/B978-0-08-102641-0.00013-X

30. Bai W, Tian X, Yao R, et al. (2020) Preparation of nano-TiO$_2$@polyfluorene composite particles for the photocatalytic degradation of organic pollutants under sunlight. *Sol Energy* 196: 616–624. https://doi.org/10.1016/j.solener.2019.12.066

31. Bai W, Yao R, Tian X, et al. (2018) Sunlight highly photoactive TiO$_2$@poly-p-phenylene composite microspheres for malachite green degradation. *J Taiwan Inst Chem E* 87: 112–116. https://doi.org/10.1016/j.jtice.2018.03.018

32. Colomer MT, Roa C, Ortiz AL, et al. (2020) Influence of Nd^{3+} doping on the structure, thermal evolution and photoluminescence properties of nanoparticulate TiO$_2$ xerogels. *J Alloy Compd* 819: 152972. https://doi.org/10.1016/j.jallcom.2019.152972

33. Pipil H, Yadav S, Chawla H, et al. (2022) Comparison of TiO$_2$ catalysis and Fenton's treatment for rapid degradation of Remazol Red Dye in textile industry effluent. *Rend Lincei-Sci Fis* 33: 105–114. https://doi.org/10.1007/s12210-021-01040-x

34. Anucha CB, Altin I, Bacaksiz E, et al. (2022) Titanium dioxide (TiO$_2$)-based photocatalyst materials activity enhancement for contaminants of emerging concern (CECs) degradation: In the light of modification strategies. *Chem Eng J Adv* 10: 100262. https://doi.org/10.1016/j.ceja.2022.100262

35. Dharma HNC, Jaafar J, Widiastuti N, et al. (2022) A review of titanium dioxide (TiO$_2$)-based photocatalyst for oilfield-produced water treatment. *Membranes* 12: 345. https://doi.org/10.3390/membranes12030345

36. Shimi AK, Ahmed HM, Wahab M, et al. (2022) Synthesis and applications of green synthesized TiO$_2$ nanoparticles for photocatalytic dye degradation and antibacterial activity. *J Nanomater* 2022: 1–9. https://doi.org/10.1155/2022/7060388

37. Bregadiolli BA, Fernandes SL, Graeff CFDO (2017) Easy and fast preparation of TiO$_2$-based nanostructures using microwave assisted hydrothermal synthesis. *Mater Res* 20: 912–919. https://doi.org/10.1590/1980-5373-mr-2016-0684

38. Dhilip Kumar R, Andou Y, Sathish M, et al. (2016) Synthesis of nanostructured Cu-WO$_3$ and CuWO$_4$ for supercapacitor applications. *J Mater Sci-Mater El* 27: 2926–2932. https://doi.org/10.1007/s10854-015-4111-z

39. Jaafar NF, Marfur NA, Jusoh NWC, et al. (2019) Synthesis of mesoporous nanoparticles via microwave-assisted method for photocatalytic degradation of phenol derivatives. *Malaysian J Anal Sci* 23: 462–471. https://doi.org/10.17576/mjas-2019-2303-10

40. Rohrer GS (2001) *Structure and Bonding in Crystalline Materials*, Cambridge University Press. https://doi.org/10.1017/CBO9780511816116

41. Pauling L (1960) The nature of the chemical bond and the structure of molecules and crystals: An introduction to modern structural chemistry, *George Fisher Baker nonresident lectureship in chemistry at Cornell University*, 3 Eds., Ithaca: Cornell University Press.

42. Galasso FS (1970) Structure and properties of inorganic solids, In: Francis S. Galasso. Illustrated by W. Darby. Pergamon Press Oxford, New York, 1st ed edition.

43. Papadaki D, Mhlongo GH, Motaung DE, et al. (2019) Hierarchically porous Cu-, Co-, and Mn-doped platelet-like ZnO nanostructures and their photocatalytic performance for indoor air quality control. *ACS Omega* 4: 16429–16440. https://doi.org/10.1021/acsomega.9b02016

44. Amreetha S, Dhanuskodi S, Nithya A, et al. (2016) Three way electron transfer of a C–N–S tri doped two-phase junction of TiO$_2$ nanoparticles for efficient visible light photocatalytic dye degradation. *RSC Adv* 6: 7854–7863. https://doi.org/10.1039/C5RA25017J

45. Belekbir S, el Azzouzi M, el Hamidi A, et al. (2020) Improved photocatalyzed degradation of phenol, as a model pollutant, over metal-impregnated nanosized TiO$_2$. *Nanomaterials* 10: 996. https://doi.org/10.3390/nano10050996

46. Wilson GJ, Matijasevich AS, Mitchell DRG, et al. (2006) Modification of TiO$_2$ for enhanced surface properties: Finite ostwald ripening by a microwave hydrothermal process. *Langmuir* 22: 2016–2027. https://doi.org/10.1021/la052716j

47. El Mragui A, Logvina Y, Pinto da Silva L, et al. (2019) Synthesis of Fe- and Co-doped TiO$_2$ with improved photocatalytic activity under visible irradiation toward carbamazepine degradation. *Materials* 12: 3874. https://doi.org/10.3390/ma12233874

48. Irfan H, Racik KM, Anand S (2018) Microstructural evaluation of $CoAl_2O_4$ nanoparticles by Williamson–Hall and size-strain plot methods. *J Asian Ceram Soc* 6: 54–62. https://doi.org/10.1080/21870764.2018.1439606

49. Ghasemifard M, Abrishami ME, Iziy M (2015) Effect of different dopants Ba and Ag on the properties of $SrTiO_3$ nanopowders. *Result Phys* 5: 309–313. https://doi.org/10.1016/j.rinp.2015.10.005

50. Nath D, Singh F, Das R (2020) X-ray diffraction analysis by Williamson–Hall, Halder–Wagner and size-strain plot methods of CdSe nanoparticles—a comparative study. *Mater Chem Phys* 239: 122021. https://doi.org/10.1016/j.matchemphys.2019.122021

51. Dey PCh, Sarkar S, Das R (2020) X-ray diffraction study of the elastic properties of jagged spherical CdS nanocrystals. *Mater Sci-Poland* 38: 271–278. https://doi.org/10.2478/msp-2020-0032

52. Rabiei M, Palevicius A, Monshi A, et al. (2020) Comparing methods for calculating nano crystal size of natural hydroxyapatite using X-ray diffraction. *Nanomaterials* 10: 1627. https://doi.org/10.3390/nano10091627

53. Gao X, Zhou B, Yuan R (2015) Doping a metal (Ag, Al, Mn, Ni and Zn) on TiO_2 nanotubes and its effect on Rhodamine B photocatalytic oxidation. *Environ Eng Res* 20: 329–335. https://doi.org/10.4491/eer.2015.062

54. Lee H-M, Kang H-R, An K-H, et al. (2013) Comparative studies of porous carbon nanofibers by various activation methods. *Carbon Lett* 14: 180–185. https://doi.org/10.5714/CL.2013.14.3.180

55. Moradi H, Eshaghi A, Hosseini SR, et al. (2016) Fabrication of Fe-doped TiO_2 nanoparticles and investigation of photocatalytic decolorization of reactive red 198 under visible light irradiation. *Ultrason Sonochem* 32: 314–319. https://doi.org/10.1016/j.ultsonch.2016.03.025

56. Iqbal A, Ibrahim NH, Rahman NRA, et al. (2020) ZnO surface doping to enhance the photocatalytic activity of lithium titanate/TiO_2 for methylene blue photodegradation under visible light irradiation. *Surfaces* 3: 301–318. https://doi.org/10.3390/surfaces3030022